The Astrophysical Journal, 624:808–820, 2005 May 10

TRIGGERED STAR FORMATION IN THE ORION BRIGHT-RIMMED CLOUDS

Hsu-Tai Lee,[1] W. P. Chen,[1,2] Zhi-Wei Zhang,[1] and Jing-Yao Hu[3]

Received 2004 September 22; accepted 2005 January 21

ABSTRACT

We have developed an empirical and effective set of criteria, based on the Two Micron All Sky Survey (2MASS) colors, to select candidate classical T Tauri stars (CTTSs). This provides a useful tool to study the young stellar population in star-forming regions. Here we present our analysis of the bright-rimmed clouds (BRCs) B35, B30, IC 2118, LDN 1616, LDN 1634, and Ori East to show how massive stars interact with molecular clouds to trigger star formation. Our results support the radiation-driven implosion model, in which the ionization fronts from OB stars compress a nearby cloud until the local density exceeds the critical value, thereby inducing the cloud to collapse to form stars. We find that only BRCs associated with strong *IRAS* 100 μm emission (a tracer of high density) and Hα emission (a tracer of ionization fronts) show signs of ongoing star formation. Relevant timescales, including the ages of O stars, expanding H II regions, and the ages of CTTSs, are consistent with sequential star formation. We also find that CTTSs are only seen between the OB stars and the BRCs, with those closer to the BRCs being progressively younger. There are no CTTSs leading the ionization fronts, i.e., within the molecular clouds. All of these findings provide strong evidence of triggered star formation and show the major roles massive stars play in sustaining the star-forming activities in the region.

Subject headings: ISM: clouds — ISM: molecules — stars: formation — stars: pre–main-sequence

1. INTRODUCTION

Young stars tend to form in clusters or groups. A giant molecular cloud may collapse and fragment to form stars of different masses. The formation of massive stars has an immense impact on the environments in which they form. On the one hand, stellar winds and shock waves from a supernova explosion may squeeze molecular clouds and induce a subsequent birth of stars that otherwise may not have occurred. On the other hand, the agitation may be so violent as to disperse the material, hindering further star formation activity. Triggered star formation (see Elmegreen 1998 for a comprehensive review)—as opposed to spontaneous cloud collapse—would have profound consequences in terms of stellar population, chemical homogeneity, star formation efficiency, and cloud energetics.

While the OB and young low-mass member stars are often distributed cospatially, in some cases low-mass pre–main-sequence (PMS) stars are seen to be located between the molecular cloud and the cluster. Such a configuration can result from either triggered or spontaneous star formation. In the former case, high-mass stars form in dense molecular cores, and then their UV photons create an expanding Strömgren sphere. The expanding ionization fronts (I-fronts) then compress nearby molecular clouds and trigger the formation of next-generation PMS stars at the edge of clouds. Alternatively, star formation may proceed in a spontaneous way; that is, all stars form coevally, but high-mass stars photoionize the surrounding clouds to expose the low-mass stars.

The Orion complex is an active star-forming region with a wealth of star-forming signatures, such as high-mass star clusters, OB associations, low-mass young stars, giant molecular clouds, reflection nebulae, and H II regions. Because of its proximity, at $\sim$450 pc, it is a suitable laboratory for the study of star formation, especially for the interplay among high-mass stars, low-mass stars, and the interstellar medium.

Bright-rimmed clouds (BRCs) are usually found at the boundary of H II regions and the edge of molecular clouds. The morphology of a BRC (e.g., tightly curved or cometary rims with tails) is governed by the I-fronts from nearby OB stars, which compress the head of the BRC, hence making the density of the apex higher than the other parts of the cloud. The imprints of such causality make it possible to delineate the intricate processes of sequential star formation. Sugitani et al. (1991) and Sugitani & Ogura (1994) catalog 89 BRCs associated with *IRAS* point sources in both the northern and southern hemispheres, some of which are also associated with Herbig-Haro objects and molecular outflows. These BRCs are potential sites in which triggered star formation might have taken place. Karr & Martin (2003) present a multiwavelength study of triggered star formation in the W5 H II region. They find some young stellar objects around W5 and suggest that the expanding H II region has induced star formation in the surrounding molecular clouds.

This paper provides an observational diagnosis to identify PMS stars from their characteristic near-infrared colors. In particular, PMS stars associated with BRCs in the Orion star-forming region are used as a tool to chronologize the star formation history to show how massive stars trigger star formation processes in the region.

We describe in § 2 our methodology in the selection of the PMS sample in parts of the Orion and Monoceros star-forming regions. In § 3 we discuss how our data lend supportive evidence of triggered star formation in the Orion BRCs. The conclusions are summarized in § 4.

2. SELECTION OF YOUNG STELLAR SAMPLE

Weak-line T Tauri stars (WTTSs) are known to emit copious X-ray emission, and a majority of them have been identified by optical spectroscopic observations of strong X-ray sources (see

[1] Institute of Astronomy, National Central University, 300 Jungda Road, Jungli City, Taoyuan 320, Taiwan; eridan@astro.ncu.edu.tw, wchen@astro.ncu.edu.tw.
[2] Department of Physics, National Central University, 300 Jungda Road, Jungli City, Taoyuan 320, Taiwan.
[3] National Astronomical Observatories, Chinese Academy of Sciences, 20A Datun Road, Chaoyang District, Beijing 100012, China.

Feigelson & Montmerle 1999 for a review). In comparison, classical T Tauri stars (CTTSs) are at earlier evolutionary stages, before much of the circumstellar material has been dispersed. CTTSs show characteristic strong IR excess emission, particularly at mid-infrared wavelengths, and Hα emission (equivalent width >5 Å). The IR excess is believed to originate from heated circumstellar dust, whereas the Hα emission comes from an active chromosphere and the boundary layer between the young star and the fast-rotating circumstellar disk. As young stars evolve and gradually clear away the surrounding material, they show different amounts of IR excesses—hence their near-infrared colors (Lada & Adams 1992). Our PMS candidates have been selected on the basis of their near-infrared colors.

2.1. *2MASS and Other Data*

This project started in early 2003, when we used the Two Micron All Sky Survey (2MASS) Second Incremental Data Release to identify CTTS candidates in the Orion and Monoceros regions. Since the 2MASS release of All Sky Data in 2003 March, we updated the photometry of our sample accordingly. The 2MASS database provides unbiased photometry in the near-infrared J (1.25 μm), H (1.65 μm), and K_S (2.17 μm) bands to a limiting magnitude of 15.8, 15.1, and 14.3, respectively, with a signal-to-noise ratio (S/N) greater than 10. The comprehensive database offers a good opportunity to identify in a systematic way young star candidates associated with molecular clouds. We use known WTTSs (Wichmann et al. 1996), CTTSs (Herbig & Bell 1988), and Herbig Ae/Be stars (Thé et al. 1994) as our template to select PMS candidates. These lists of WTTSs, CTTSs, and Herbig Ae/Be stars, taken from the literature and not confined to any special region in the sky, serve as a compilation of their descriptive 2MASS colors. Figure 1 plots the $J - H$ versus $H - K_S$ color-color diagram extracted from the 2MASS catalog for these PMS stars. Only sources with high-S/N photometry are included. The fact that the CTTS, WTTS, and Herbig Ae/Be stellar populations appear to occupy different regions in Figure 1 enables us to pick out candidate PMS stars. The 2MASS database, as a rule with simultaneous measurements in all three bands, is particularly useful as a diagnostic of young stellar population based on colors because a majority of PMS stars are variables.

Also shown in Figure 1 is the locus for main-sequence stars, for which the WTTSs are seen to follow. The CTTSs are found to lie approximately between the two parallel dotted lines, defined empirically by $(j\_m - h\_m) - 1.7(h\_m - k\_m) + 0.0976 = 0$ and $(j\_m - h\_m) - 1.7(h\_m - k\_m) + 0.450 = 0$, where j_m, h_m, and k_m are 2MASS magnitudes, and the slope is specified by the interstellar reddening law (Rieke & Lebofsky 1985). The dashed line in Figure 1 represents the dereddened CTTS locus (Meyer et al. 1997), modified to the 2MASS photometry (Carpenter 2001), with $(j\_m - h\_m) - 0.493(h\_m - k\_m) - 0.439 = 0$. The dotted parallel lines separate CTTSs from Herbig Ae/Be and from reddened main-sequence stars. The fact that different kinds of PMS stars occupy separate regions in the $J - H$ versus $H - K_S$ color-color diagram enables us to identify candidate young stars in star-forming regions. We select 2MASS point sources with colors between the two parallel lines and above the dashed line as CTTS candidates. Inevitably, our selection misses some CTTSs to the left of the parallel lines, where slightly reddened CTTSs and reddened main-sequence stars cannot be distinguished by their 2MASS colors. This poses no difficulty for our study because our goal is not to collect a complete PMS sample but to use young stars as probes of the star formation history in the region. Data at longer wavelengths, e.g., in the L band and beyond, would serve to better discriminate between moderately reddened CTTSs and reddened main-sequence stars (Lada et al. 2000).

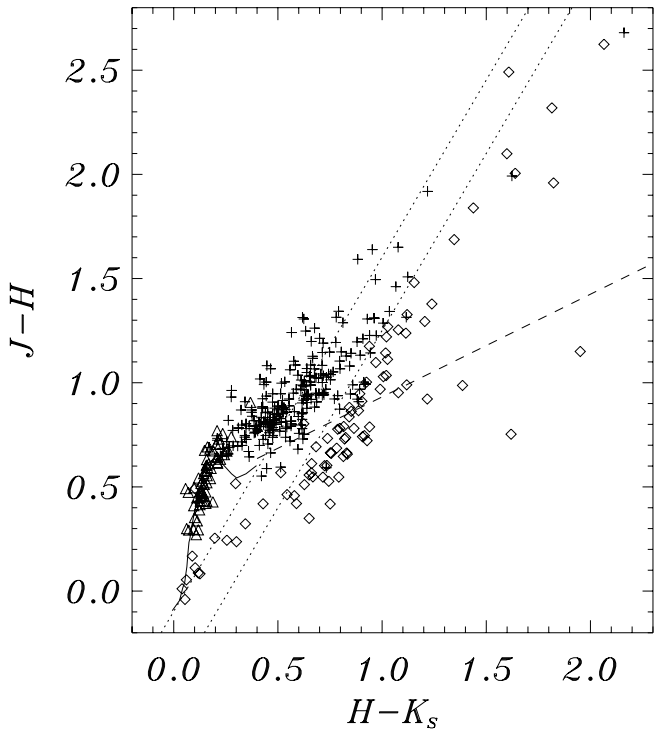

FIG. 1.—2MASS *JHK* color-color diagram for known WTTSs (Wichmann et al. 1996; *triangles*), CTTSs (Herbig & Bell 1988; *plus signs*), and Herbig Ae/Be stars (Thé et al. 1994; *diamonds*). The solid line is the main-sequence locus. The two dotted parallel lines, with the slope derived from interstellar reddening law (Rieke & Lebofsky 1985), separate CTTSs from Herbig Ae/Be and from reddened main-sequence stars. The dashed line is the dereddened CTTS locus (Meyer et al. 1997).

To improve photometric accuracy and remove extended sources from the 2MASS Point Source Catalog, we have set further criteria for selecting our CTTS candidates. These may be useful to other users of the 2MASS data, so we summarize them in Table 1. The photometric quality flag (ph_qual = AAA) indicates a S/N $\geq$ 10 and a corrected photometric uncertainty <0.10857 mag, which is an indication of the best-quality detection in terms of photometry and astrometry. The blend flag (bl_flg) = 111 implies no source blending; the contamination and confusion flag (cc_flg) = 000 means that the source is unaffected by known artifacts or that no artifact is detected in the band. Only sources without a neighboring star within 5″ (prox > 5.″0) are considered, so as to avoid possible photometric confusion. We selected only sources that have optical counterparts ($a \neq 0$) and identified CTTS candidates according to their near-IR colors, as described in the last paragraph.

Some slightly extended sources may be included in the 2MASS Point Source Catalog, notably, nuclei of galaxies. In order to single out these nonstellar sources, additional criteria have been imposed. An extended source can be discriminated from a point source by the difference between its measured fluxes determined with a point-spread function (PSF) fitting and with aperture photometry. Conceivably, an extended source measured by PSF photometry would lose some flux at the outer image halo. The 2MASS entries, [*jhk_m*], are default magnitudes mostly derived from PSF fitting, whereas the entries identified as [*jhk_m_stdap*] are standard aperture magnitudes derived from 4″ radius photometric aperture. Therefore, the parameter $(j\_m - j\_m\_stdap) + (h\_m - h\_m\_stdap) + (k\_m - k\_m\_stdap)$ should be close to 0

TABLE 1
SELECTION CRITERIA OF CTTSs FROM THE 2MASS POINT SOURCE CATALOG

Criterion	Description
Photometric quality flag (*ph_qual*) = AAA	S/N $\geq$ 10 and [*jhk*]_*cmsig* $<$ 0.10857 for best-quality detections in photometry and astrometry
Blend flag (*bl_flg*) = 111	No source blending
Contamination and confusion flag (*cc_flg*) = 000	Source unaffected by known artifacts
Proximity (prox) > 5.″0	Photometry not confused by nearby objects
Minor Planet Flag (*mp_flg*) = 0	Not a minor planet
(*j_m* − *j_m_stdap*) + (*h_m* − *h_m_stdap*) + (*k_m* − *k_m_stdap*) $\leq$ 0.3 mag	To distinguish an extended source from a point source
(*j_m* − *h_m*) − 1.7(*h_m* − *k_m*) + 0.0976 $\leq$ 0	2MASS colors of CTTSs
(*j_m* − *h_m*) − 1.7(*h_m* − *k_m*) + 0.4500 $\geq$ 0	
(*j_m* − *h_m*) − 0.493(*h_m* − *k_m*) − 0.439 $\geq$ 0	
Optical counterpart ($a \neq 0$)	With an optical counterpart
Signal-to-noise ratio ([*jhk*]_*snr*) > 30	S/N > 30

for point sources and significantly nonzero for extended objects. We set (*j_m* − *j_m_stdap*) + (*h_m* − *h_m_stdap*) + (*k_m* − *k_m_stdap*) $\leq$ 0.3 as our selection criterion. Finally, we choose sources with S/N greater than 30 ([*jhk*]_*snr* > 30) for high-quality photometry. These stringent criteria do bias against sources in crowded regions, but, as shown below, they prove to lead to a high success rate in selection of CTTS candidates.

In addition to 2MASS, we have made use of other survey data, such as Hα (Finkbeiner 2003; Gaustad et al. 2001), $E(B-V)$ reddening (Schlegel et al. 1998), and *IRAS* 100 μm emission in the Orion star-forming region, to trace, respectively, the distribution of ionization fronts, cloud extinction, and IR radiation with respect to the spatial distribution of our sample of young stars.

2.2. *Spectroscopic Observations*

To justify the selection criteria outlined above, we chose 32 relatively bright CTTS candidates for spectroscopic observations to check that they are indeed young sources. Low-dispersion spectra, with a dispersion of 200 Å mm^{-1}, 4.8 Å pixel^{-1}, were taken with the 2.16 m optical telescope of the Beijing Astronomical Observatory on 2003 January 22, 23, 30, and 31. An OMR (Optomechanics Research, Inc.) spectrograph was used with a Tektronix 1024 $\times$ 1024 CCD detector covering 4000–9000 Å. The data were processed with standard NOAO/IRAF packages. After the bias and flat-fielding corrections, the IRAF package KPNOSLIT was used to extract each spectrum and to calibrate its respective wavelength and flux. Table 2 lists the results of our spectroscopic observations. The first column gives the sequence number. Columns (2)–(5) list the 2MASS identification and photometry. Columns (6)–(9) are, respectively, spectral type, the associated star-forming region, forbidden line(s) in the spectrum, if any, and other names for the source. We note that stars 3, 5, 6, 14, 15, 16, 20, 21, 22, and 24 in Table 2 show continuous or veiled spectra with [O I] and/or [S II] emission lines (Fig. 2), which are characteristics of the extreme T Tauri stars commonly seen in Class I sources in which the forbidden lines originate from jets or winds (Kenyon et al. 1998).

These 32 candidates, distributed in the range R.A. $\sim 5^{\rm h}$–$6^{\rm h}$ covering part of the Orion and part of the Monoceros star-forming regions, have been chosen somewhat randomly. Our spectroscopic observations show that 24 of the 32 candidates are found indeed to be pre–main-sequence stars, with 4 of the others appearing as M-type stars and 4 as carbon stars. All 24 confirmed PMS stars are associated with star-forming regions, but otherwise the M stars and carbon stars are scattered around the region. This indicates that our criteria used to select PMS stars from the 2MASS database are valid and very effective. If the same set of criteria is applied to sources seen against nearby molecular clouds—as is the case here in Orion and Monoceros BRCs—for which both background and foreground field-star contamination is small, the success rate should be conceivably even higher.

Figure 3 shows the color-magnitude and color-color diagrams of the 24 spectroscopically confirmed CTTSs in Table 2. Stars with and without forbidden lines are denoted with different symbols. In the color-magnitude diagram (CMD), the stellar absolute J magnitude, as the ordinate, is derived by adopting a distance of 450 pc to the Orion clouds and a distance of 830 pc to the Mon R2 and LDN 1652 star-forming regions (Maddalena et al. 1986). One sees that in either the CMD or the color-color diagram, the CTTSs with forbidden lines are systematically farther away from the zero-age main sequence (ZAMS), implying that the CTTSs with forbidden lines are younger than those without.

This result, that younger CTTSs are located toward the upper right corner in the near-infrared color-color diagram, is consistent with that obtained by Lada & Adams (1992). Class I sources with very red colors, $J-H > 1.8$ mag, are located even more toward the upper right corner in the diagram. In contrast, the WTTSs are close to the main-sequence locus, whereas the CTTSs occupy a region between those of the Class I sources and the WTTSs. This is understood as an evolutionary sequence; that is to say, a young star evolves in such a color-color diagram from the upper right to lower left in a sequence from a Class I protostar to a CTTS with forbidden lines, to a CTTS without forbidden lines, and eventually to a WTTS.

The spectroscopic observations demonstrate that our selection of PMS sample on the basis of 2MASS colors is reliable and that the CMD and color-color diagram can be used, particularly for those CTTSs that are too faint for us to obtain their spectra, to diagnose their evolutionary status. We are now ready to use these tools to identify a sample of PMS stars in star-forming clouds, which in turn allows us to probe the star formation activity and history in the region.

3. EVIDENCE OF TRIGGERED STAR FORMATION

We present the analysis of the PMS population in relation to the bright-rimmed molecular clouds and massive stars to investigate how triggered star formation might have taken place. This paper concentrates on the Orion BRCs, IC 2118, LDN 1616, LDN 1634, and perhaps also Ori East, associated with the Trapezium, and B30 and B35 associated with λ Ori (Fig. 4). The sample used in this study consists of (1) 33 CTTS candidates (including 2

TABLE 2
SPECTROSCOPIC OBSERVATIONS OF YOUNG STAR CANDIDATES

Star (1)	2MASS (2)	J (mag) (3)	H (mag) (4)	K_S (mag) (5)	Sp. Type[a] (6)	Region (7)	Forbidden Lines[b] (8)	Other Name (9)
1.....	J05350900−0427510	10.797	10.109	9.634	K0	Orion A	...	(R2001) 1754
2.....	J05353672−0510004	13.309	12.481	11.936	M3	Orion A	...	(AD 95) 1868
3.....	J05385149−0801275	12.967	11.525	10.513	M5	Orion A	O, S	
4.....	J05402496−0755353	12.446	11.367	10.658	M4	Orion A	...	
5.....	J05412534−0805547	10.604	9.824	9.287	Cont.	Orion A	O	HBC 181
6.....	J05412771−0931414	12.147	11.033	10.272	Cont.	Orion A	O	Kiso A-1048 45
7.....	J05423584−0958552	9.973	8.959	8.227	Cont.	Orion A	...	
8.....	J05432701−0959375	10.984	10.166	9.542	K5	Orion A	...	
9.....	J05342764−0457051	13.737	12.890	12.286	M2	Orion A	...	(CHS 2001) 3990
10.....	J05342978−0451477	13.241	11.781	10.910	K7	Orion A	...	(CHS 2001) 4167
11.....	J05122053−0255523	10.425	9.688	9.140	K3	...	...	V531 Ori
12.....	J05371885−0020416	11.577	10.761	10.263	K5	...	...	Kiso A-0904 58
13.....	J06014515−1413337	11.698	10.896	10.211	K5	...	...	IRAS 05594−1413
14.....	J05073016−0610158	10.822	9.572	8.611	M0	IC 2118	O, S	
15.....	J05073060−0610597	10.120	9.040	8.251	M2	IC 2118	O	
16.....	J05202573−0547063	11.036	10.202	9.608	Cont.	LDN 1634	O, S	V534 Ori
17.....	J06075243−0516036	10.417	9.474	8.639	K0	Mon R2		HBC 518
18.....	J06075463−0614342	11.676	10.851	10.094	K0	Mon R2	...	
19.....	J06080003−0519022	11.384	10.413	9.649	K0	Mon R2	...	
20.....	J06261259−1028346	12.412	11.352	10.487	Cont.	LDN 1652	O, S	
21.....	J06265529−0958014	11.914	10.901	10.126	Cont.	LDN 1652	O	
22.....	J06265731−0959395	13.161	12.137	11.363	Cont.	LDN 1652	O	
23.....	J06273428−1002397	12.522	11.737	11.176	K7	LDN 1652	...	
24.....	J06280028−1003420	12.006	10.935	10.091	Cont.	LDN 1652	O	
25.....	J05375005−1548114	6.573	5.571	4.912	M9	...	...	IRAS 05355−1549
26.....	J06222376−0255509	10.410	8.734	7.559	C	...	...	IRAS 06198−0254
27.....	J06380179−0557170	8.000	6.711	5.841	C	...	...	
28.....	J06270654−0540512	8.082	6.751	5.882	C	...	...	
29.....	J06160006−1727270	10.213	8.978	8.040	C	...	...	
30.....	J06265037−0738456	9.830	8.845	8.543	M2	...	...	
31.....	J05345877−0928274	7.700	6.818	6.295	M9	...	...	V653 Ori
32.....	J05413322−0755022	12.209	11.174	10.526	M2	...	...	Haro 4-488

[a] Cont.: continuum spectra; C: carbon star.
[b] O–[O I]; S–[S II].

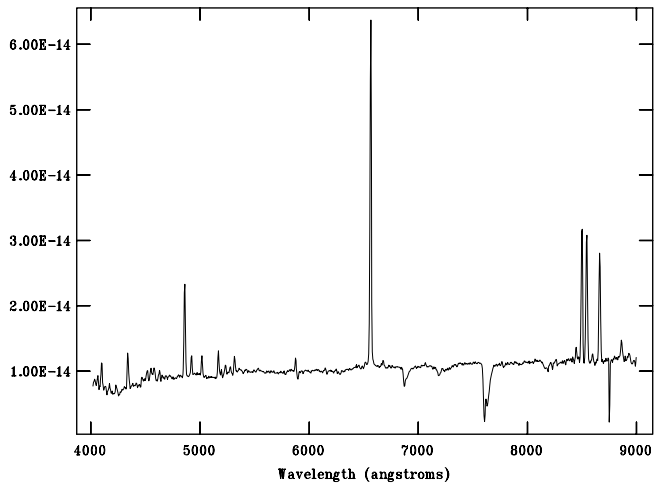

FIG. 2.—Example CTTS spectrum for star 16 showing extreme CTTS characteristics of a veiled continuum with strong Hα, Ca II triplets, and forbidden [O I] and [S II] lines.

confirmed CTTSs in IC 2118 and one in LDN 1634; see Table 2) around the Trapezium, in the region from R.A. $\sim 5^h$ to 5^h30^m and from decl. $\sim -2^\circ$ to -9°, and (2) 18 CTTS candidates around λ Ori, in R.A. $\sim 5^h25^m$ to 5^h50^m and decl. $\sim +8^\circ$ to $+14^\circ$.

IC 2118, LDN 1616, and LDN 1634 are isolated molecular clouds to the west of the Orion A and are part of the Orion star-forming region. The three molecular clouds are all associated with strong *IRAS* 100 μm emission and are apparently engraved by the UV radiation from the Trapezium, with bright-rimmed boundaries outlined by Hα filaments, which are presumably shaped by the I-fronts (Fig. 5). We differentiate the CTTSs that are physically close to the BRCs from those farther away, as marked in Figure 5.

The spectra of stars 14, 15, and 16, associated with IC 2118 and LDN 1634, all exhibit forbidden lines, [S II] and/or [O I], suggestive of youth. The spatial distribution of these CTTSs likely traces a preexisting molecular cloud complex from which IC 2118, LDN 1616, and LDN 1634 are merely survivors.

LDN 1621 and LDN 1622, also called Ori East (Herbig & Rao 1972), are at about the same distance as Orion B (Maddalena et al. 1986). Interaction between the Ori East clouds and the I-front can be seen in Figure 6.

B30 and B35 are associated with S264, an extended H II region excited by the O8 III star λ Ori and surrounded by but slightly

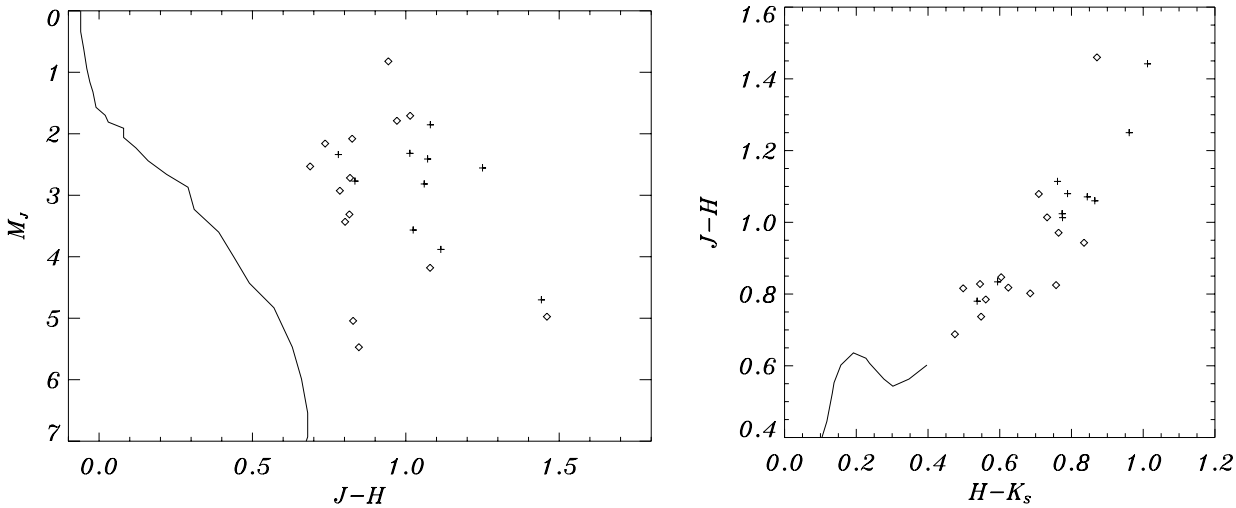

FIG. 3.—CMD (*left*) and color-color diagram (*right*) for the 24 verified CTTSs in Table 2 with (*plus signs*) and without (*diamonds*) optical forbidden lines. In the CMD the solid line represents the ZAMS. In the color-color diagram the solid line is the main-sequence locus. In either case, the CTTSs with forbidden lines are farther away from the main sequence, which is suggestive of their redder colors and younger ages than those without forbidden lines.

off-center from a ring molecular cloud (Lang et al. 2000). Duerr et al. (1982) surveyed about 100 deg^2 around λ Ori and found 83 Hα emission-line stars, mostly distributed along a barlike structure extending on either side from λ Ori to B30 and to B35. These authors suggest that the Hα stars provide a fossil record of a preexisting giant molecular cloud complex. Dolan & Mathieu (2002) identified PMS stars in the region around λ Ori by statistically removing field stars in the optical CMD. The seeming lack of the youngest (1–2 Myr) PMS stars inside the molecular ring, despite the apparent abundance of such stars in B30 and B35, leads Dolan & Mathieu (2002) to postulate a possible supernova explosion near λ Ori that terminated recent star formation in the vicinity. The CTTS candidates we have identified are spread along the barlike structure, but they lie clearly within

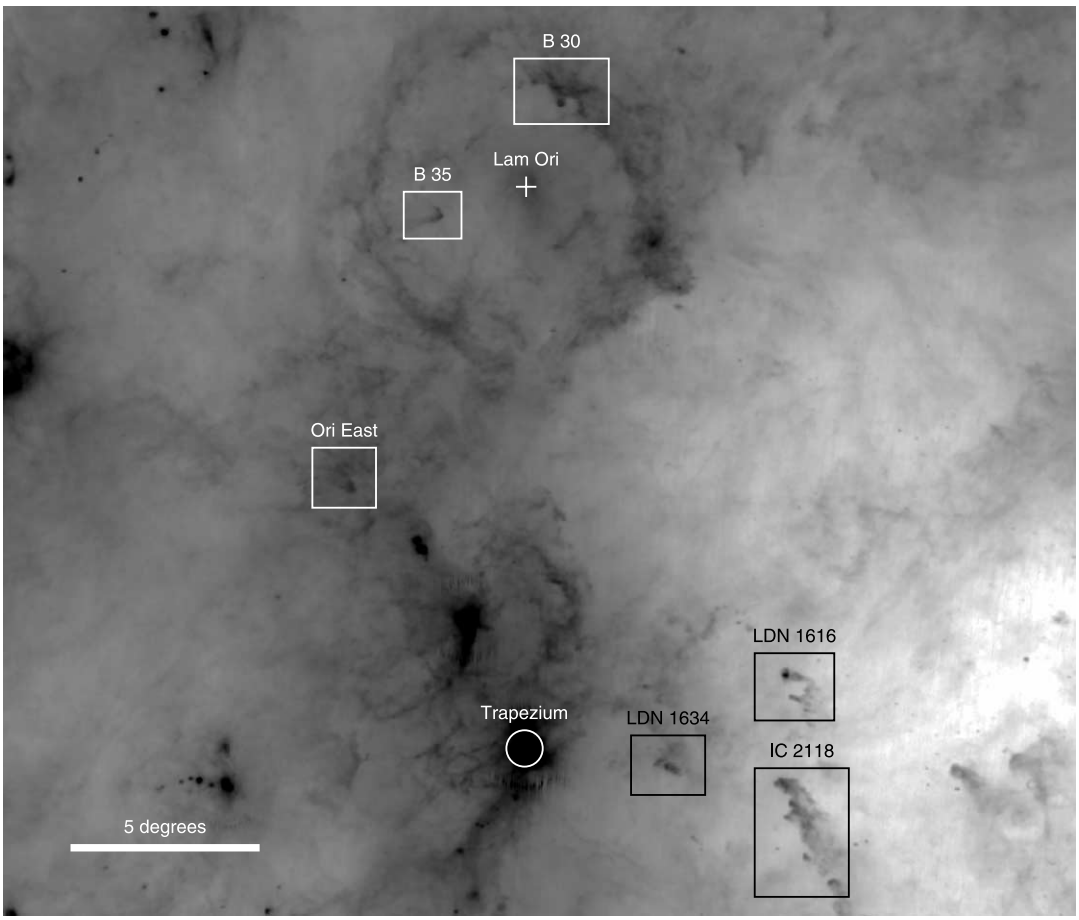

FIG. 4.—*IRAS* 100 μm image of the Orion region with the six bright-rimmed clouds studied in this work, B30, B35, Ori East, LDN 1616, LDN 1634, and IC 2118.

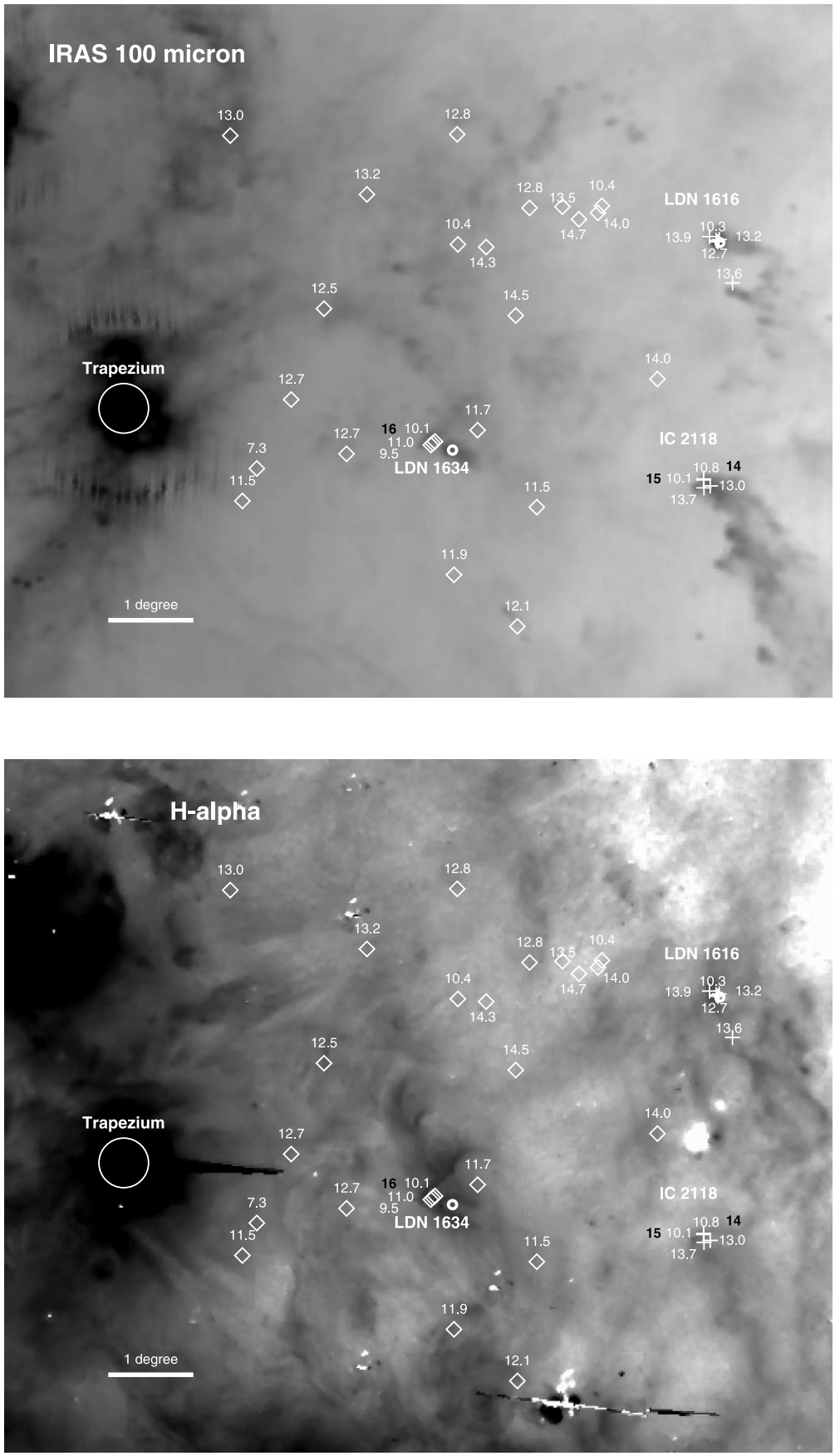

FIG. 5.—*IRAS* 100 μm and Hα images in IC 2118, LDN 1616, and LDN 1634. There are a total of 33 CTTS candidates in the region. The plus signs denote those CTTSs physically closer to the BRCs, and the diamonds are those farther away, with the *J*-band magnitude labeled for each star. Stars 14, 15, and 16 in Table 2 are labeled in black. The circles mark the positions of known protostars in the clouds (see § 3.2).

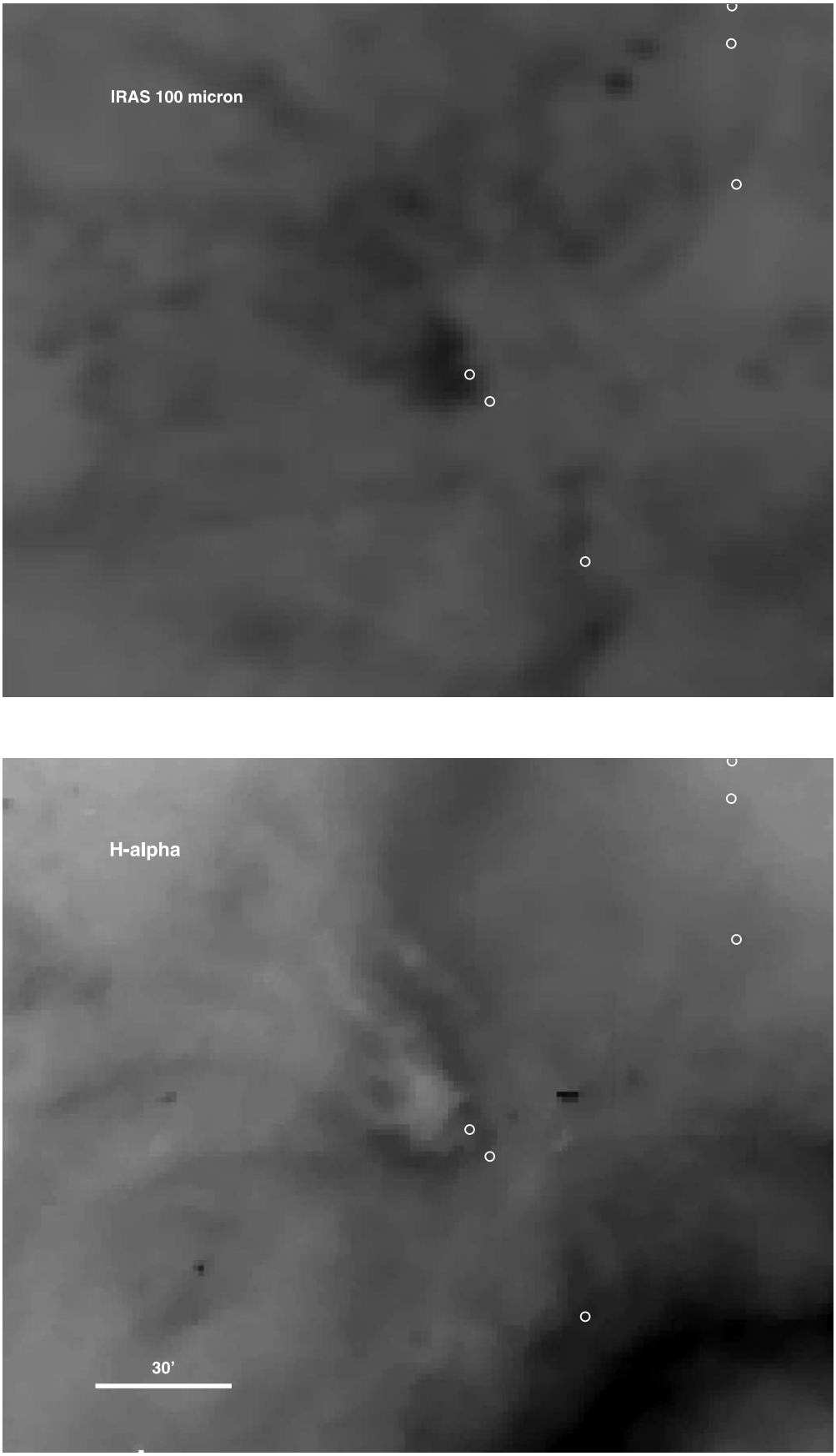

FIG. 6.—*IRAS* 100 μm and Hα images of Ori East, with candidate CTTSs marked.

the central cavity previously thought to be free of ongoing star-forming activities. Prominent Hα and *IRAS* 100 μm emission are seen in both B30 and B35 on the sides facing λ Ori (Fig. 7), signifying the interaction between λ Ori and these two BRCs.

3.1. *Comparison with Theory*

The radiation-driven implosion (RDI) model, based on the "rocket effect," proposed by Oort & Spitzer (1955) and further developed by Bertoldi (1989) and Bertoldi & McKee (1990), links BRCs to PMS stars. The UV photons from massive stars ionize the outer layers of a nearby cloud, which expand to the surrounding medium with an I-front speed $\sim$10 km s^{-1}. The expanding I-front plows the cloud material, which, when it exceeds the local critical mass, collapses to form new stars. There are two phases, namely, the collapsing and cometary phases, in the formation and evolution of a cometary globule (Lefloch & Lazareff 1994, 1995; Lefloch et al. 1997). In the initial collapsing phase, UV photons ionize the surface layers of a cloud, causing the cloud to elongate in the direction of the high-mass stars. This phase lasts some 10^5 yr. Subsequently, according to the model, the cloud remains in a quasi-stationary state, with small-scale condensations close to critical equilibria. If the pressure from the I-front exceeds that of the molecular cloud, the density increases to beyond the critical value and the collapse of the condensations leads to star formation, leaving behind a chain of PMS stars reminiscent of the original, elongated cloud. On the other hand, if the I-front pressure does not exceed that of the molecular gas, the I-front stalls and there should be no star formation. This cometary phase may last a few million to a few 10^7 yr. Eventually, the entire cometary globule is evaporated by the UV photons.

According to the RDI model, the surface of a BRC facing the massive stars is compressed by the I-fronts. De Vries et al. (2002) observed B35 and LDN 1634 in HCO^+ and other molecular line transitions to trace the swept-up gas ridge and overly dense regions. They find that the surfaces of B35 and LDN 1634 facing the massive stars are indeed being compressed, as the RDI model predicts.

Ogura & Sugitani (1998) listed several dozen bright-rimmed clouds, cometary globules, and reflection clouds in the Orion OB1. They propose that these present an evolutionary sequence and collectively call them "remnant molecular clouds." We find that not all remnant molecular clouds are associated with CTTSs. Instead, only those BRCs associated with prominent Hα and *IRAS* 100 μm emission, e.g., IC 2188, LDN 1616, and LDN 1634, have ongoing star formation (Fig. 8), consistent with the RDI model. The Hα filaments and the 100 μm emission trace, respectively, the I-fronts and dense regions in a molecular cloud. Obviously, in IC 2188, LDN 1616, and LDN 1634 the I-front has out-pressured the molecular clouds and thus triggered star formation. The two BRCs B30 and B35 in the vicinity of λ Ori represent two additional such examples of triggered star formation. Remnant clouds without star formation are simply the outcome of I-fronts with insufficient pressure.

The RDI model predicts the cloud to collapse perpendicular to the direction of the ionizing massive stars. This has been observed in LDN 1616 and IC 2118 by Yonekura et al. (1999), for which the ^{12}CO, ^{13}CO, and C^{18}O emission contours show elongation roughly toward the Trapezium.

3.2. *Sequential Star Formation*

Triggered star formation is a sequential process. Massive stars form first, and their I-fronts expand to nearby molecular clouds, compressing them and prompting the next-generation stars to form. The process may continue until the cloud is consumed and no more star-forming material is available. As time passes, the PMS stars line up between the massive stars and the molecular cloud, along which the stars farther away from the massive stars, and thus closer to the molecular cloud, should be progressively younger. The youngest stellar objects, namely, protostars (Class 0 and Class I objects; Lada 1987), are still embedded within the cloud.

Our data indicate a systematic brightness difference among revealed CTTSs, in the sense that brighter CTTSs are more distant from λ Ori (see Fig. 7). We consider this to be a consequence of triggered star formation. Initially, the B30 and B35 clouds might have been extended toward λ Ori, perhaps with a barlike structure (Duerr et al. 1982). The I-front from λ Ori propagates and rams through the clouds, leaving behind newborn stars. Figure 10 plots the CMD in the λ Ori region. Indeed, the CTTSs closer to B30 and B35 are progressively younger and occupy positions away from the ZAMS (Siess et al. 2000). The brightest CTTSs, close to B30 and B35, may be among the youngest, which have just revealed themselves on the birth line and begun their descent down the Hayashi tracks. The same phenomenon, namely, in which the CTTSs closer to the BRCs are perceptibly younger, is seen in LDN 1616, LDN 1634, and IC 2118 (Fig. 9). The star formation sequence is similar, except here with the Trapezium as the triggering source.

Figure 10 also shows the color-color diagram of the λ Ori region, in which the CTTSs physically closer to BRCs are located toward the upper right corner. The extinction values in these BRCs, derived from Schlegel et al. (1998), are in general too low to affect the apparent colors significantly. This implies that these CTTSs are intrinsically young. In LDN 1616, LDN 1634, and IC 2118, we likewise find results similar to those in the λ Ori region (see Fig. 9).

Some very young objects are known to exist in these regions, for example, Class 0 sources in B30 (RNO 43MM; Zinnecker et al. 1992) and in LDN 1616 (L 1616 MMS1A; Stanke et al. 2002) and Class I sources in B35 and in LDN 1634 (De Vries et al. 2002). Each of them is indeed embedded in and close to the apex of the associated cloud, as expected in the RDI model. We are apparently witnessing an ongoing star formation sequence, with the coexistence of CTTSs, younger PMS objects associated with the BRCs, and the youngest protostars embedded within the clouds.

3.3. *Relevant Timescales*

In the triggered star-formation scenario, the ages of the concurrent OB stars must be greater than the ages of the second-generation stars plus the I-front traveling time. The stars $^1\theta$ Ori A, B, C, and D, with spectral types B0.5 V, B3 V, O6:, and B0.5 V, respectively (Levato & Abt 1976), are the most massive members in the Trapezium and the main sources to create the I-fronts. The star $^1\theta$ Ori C may be somewhat peculiar in its evolutionary status (Walborn & Panek 1984), so we adopt the age of $^1\theta$ Ori A and D, both of spectral type B0.5 V and with a lifetime of 6×10^6 yr (Schaerer & de Koter 1997) to represent the ages of the OB stars.

Assuming that IC 2118, LDN 1616, and the Trapezium are at the same distance from us, IC 2118 and LDN 1616 are thus separated from the Trapezium by about 55 pc. With an I-front speed, i.e., the sound speed in an H II region, of $\sim$10 km s^{-1}, it takes some 5.5×10^6 yr for the I-front to traverse the distance between the clouds and the Trapezium. The lifetimes of CTTSs range from a few $\times 10^5$ to a few $\times 10^6$ yr. The CTTSs associated with the BRCs are younger than those outside the clouds (§ 3.2), but

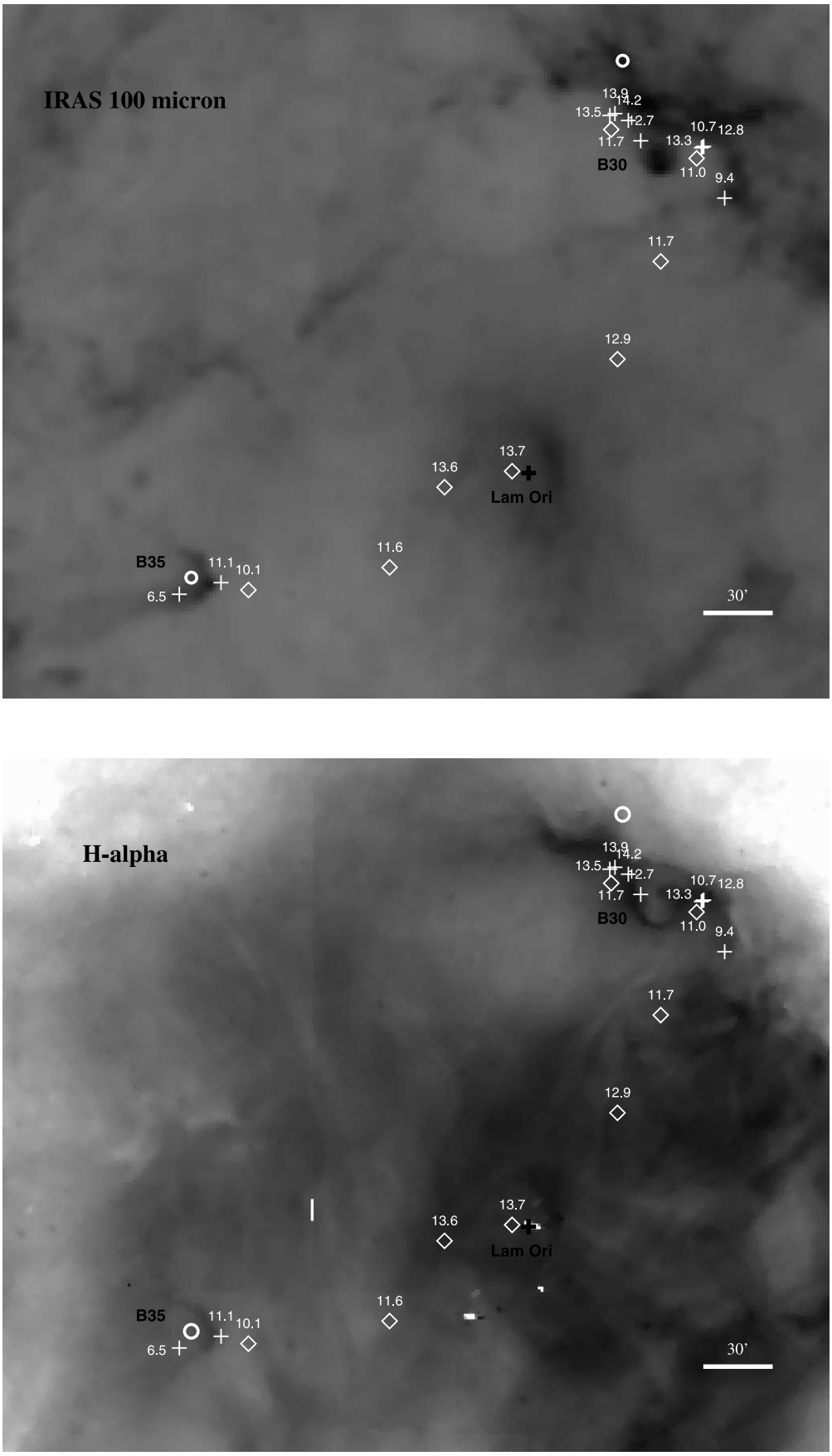

FIG. 7.—Same as Fig. 5, but for B30 and B35. There are a total of 18 CTTS candidates in the region.

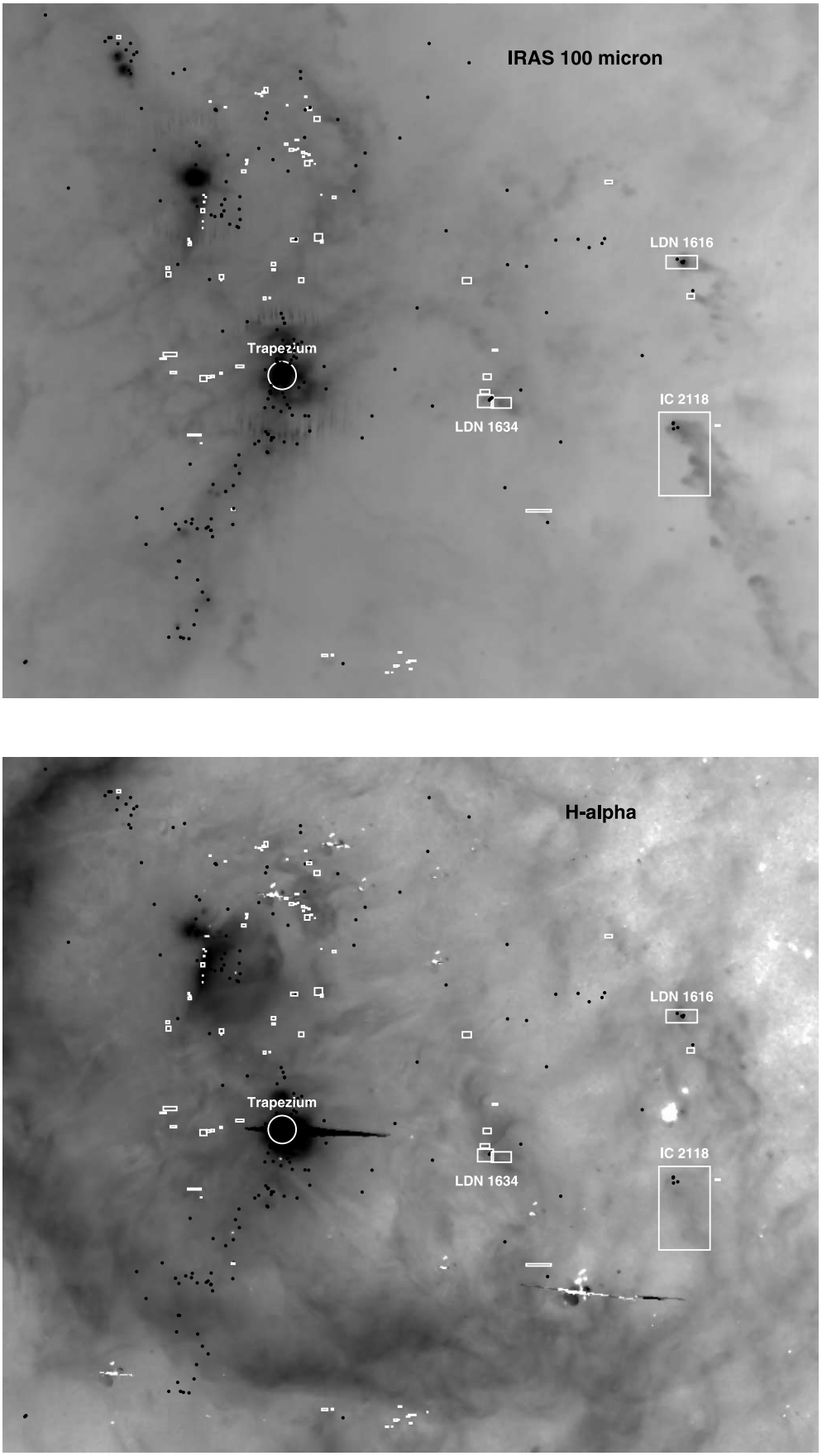

FIG. 8.—*IRAS* 100 μm and Hα images of remnant molecular clouds. The white boxes are the remnant molecular clouds (Ogura & Sugitani 1998), and the black dots symbolize the candidate CTTSs. Only clouds associated with strong IR and Hα emission are found to harbor CTTSs.

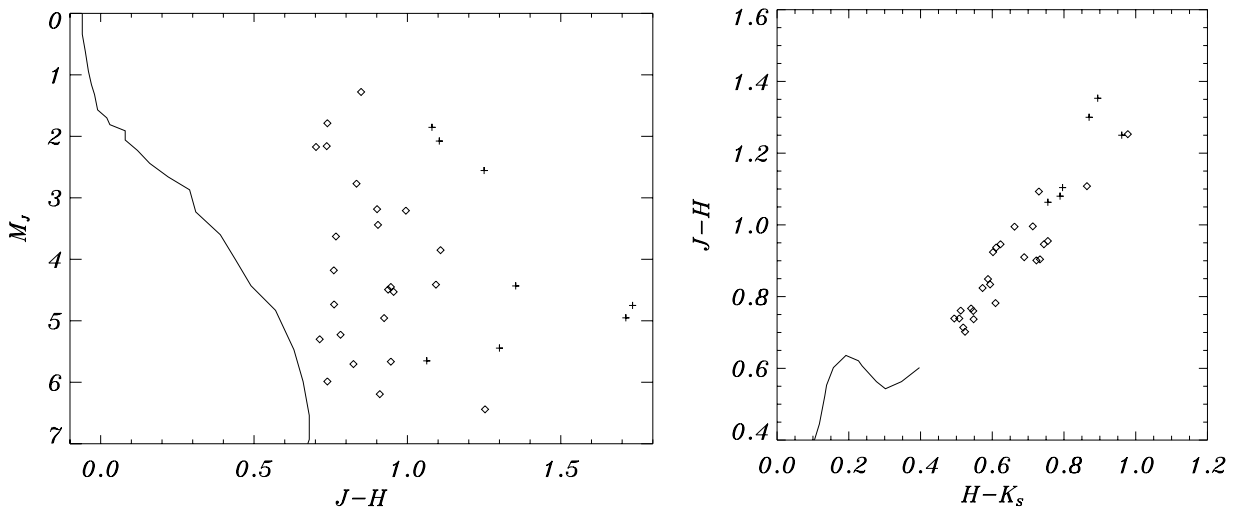

FIG. 9.—CMD (*left*) and color-color diagram (*right*) of IC 2118, LDN 1616, and LDN 1634. In the CMD the solid line represents the ZAMS. In the color-color diagram the solid line is the main-sequence locus. The CTTSs physically closer to BRCs are marked with plus signs, and those farther away are marked with diamonds (see Fig. 5).

even for the oldest CTTSs in the region, the combined timescale 6×10^6 yr is consistent with the age of the Trapezium.

Likewise, the set of timescales can be estimated for the λ Ori system, which consists of an O star and an H II region surrounded by an unusual molecular cloud ring. The radius of the molecular cloud ring is approximately 2°.6, or about 20 pc at a distance of 450 pc, so it would take about 2 Myr for the I-front originating in λ Ori to travel through the H II region. The age of λ Ori, an O8 III star with a luminosity of 340,000 $L_\odot$ and an effective temperature of 34,700 K (Schmidt-Kaler 1982), can be inferred from evolutionary tracks (Schaerer & de Koter 1997) to be about 3×10^6 yr. Here again, the age of the triggering object, λ Ori (3×10^6 yr), is consistently longer than the expanding timescale of the I-front (2×10^6 yr) plus the age of the CTTSs.

3.4. *Spatial Distribution of Classical T Tauri Stars*

The spatial distribution of CTTSs provides telltale clues as to the star formation history in a molecular cloud. According to the RDI model, small-scale condensations compressed by the I-fronts reach critical equilibria first at the surface layers of BRCs, where the CTTSs should be found. If CTTSs exist far ahead of the I-front and are still embedded in the molecular cloud, star formation must have proceeded in a spontaneous manner, i.e., the embedded CTTSs were formed at the same time as their massive counterparts. On the other hand, if CTTSs are only seen near the surfaces of (with none embedded inside of) the BRCs, triggered star formation is clearly evidenced. In B30, B35, IC 2118, LDN 1616, LDN 1634, and Ori East, CTTSs are seen only between the massive stars and BRCs and on the compressed (i.e., dense) sides of BRCs (see Figs. 5, 6, and 7). No CTTSs are found farther down the compressed regions into the molecular clouds.

To investigate whether the BRCs are indeed void of embedded PMS stars, we computed the probability of our failure to detect them, if they actually did exist, because of excessive dust extinction in the clouds. Table 3 contains the extinction of IC 2118, LDN 1616, LDN 1634, B30, and B35. Column (1) lists the five BRCs. Columns (2)–(4) are the values of $E(B-V)$, A_V, and A_J in each cloud. The values of $E(B-V)$ are derived from Schlegel et al. (1998), and $A_V/E_{B-V} = 3.1$ and $A_J = 0.282 A_V$ (Cox 2000) are used to obtain A_V and A_J. If there were CTTSs embedded in a particular cloud, the idea would be to estimate how many of them would have to have escaped detection. We created the $E(B-V)$ map (Schlegel et al. 1998) for each cloud and assumed the same

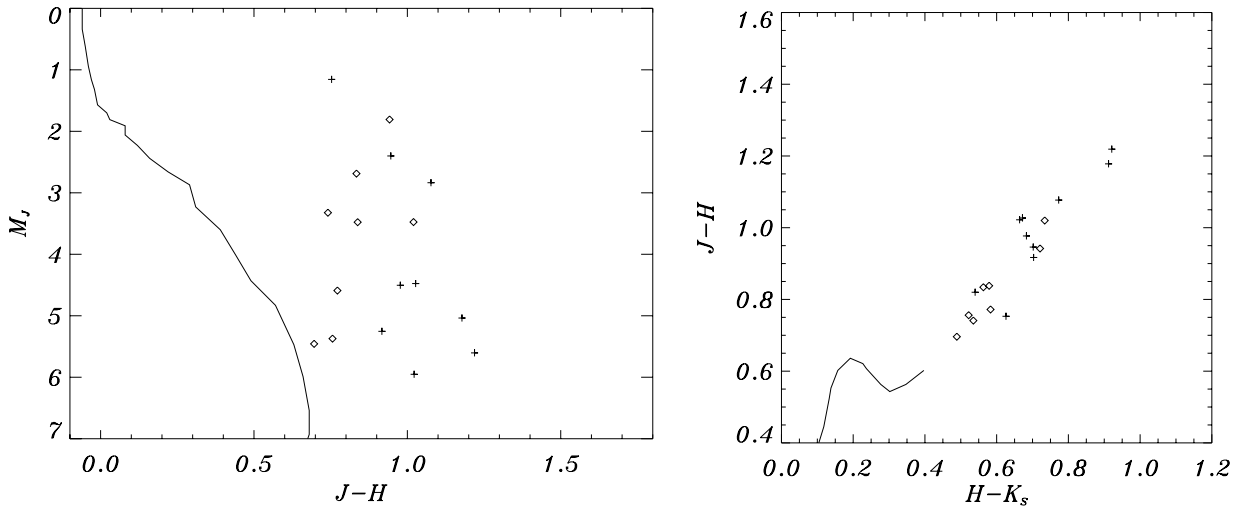

FIG. 10.—Same as Fig. 9, but for the B30 and B35 regions (see Fig. 7).

TABLE 3
Extinction of Bright-rimmed Clouds

BRC (1)	$E(B-V)$[a] (mag) (2)	A_V ($R = 3.1$) (mag) (3)	A_J (mag) (4)	Nondetection Probability (5)
IC 2118	1.1–0.2	3.4–0.6	0.96–0.17	0.021
LDN 1616.....	2.3–0.2	7.1–0.6	2.01–0.17	0.051
LDN 1634.....	1.1–0.3	3.1–0.9	0.87–0.25	0.013
B30.....	2.6–1.5	8.1–4.7	2.28–1.31	0.058
B35.....	1.3–0.5	4.0–1.6	1.14–0.44	0.001

[a] Schlegel et al. (1998).

J-band luminosities for the embedded CTTSs as for the visible CTTSs outside the cloud. We performed a Monte Carlo computation to distribute randomly the hypothetical CTTSs on the $E(B-V)$ map to check their detectability, given the 2MASS detection limit of $J = 15.0$ (S/N = 30), based on selection criteria discussed in § 2. The probability of nondetection of embedded CTTSs in each cloud is given in column (5). As can be seen, the probability of CTTSs that would have escaped our detection is universally very low, <0.06, implying that the extinction in these clouds is too low to make any embedded PMS stars invisible. In other words, if there were any embedded sources, we would have detected them. We conclude, therefore, that the CTTSs near the surfaces of the BRCs are not part of a young stellar population originally embedded in the molecular clouds and later revealed by UV photons from massive stars. They are relics of triggered star formation.

Most PMS stars are associated with molecular clouds, but some are distinctly away from any clouds. These isolated PMS stars, with their young age, could not have traversed from their birthplace to their current positions. They are revealed as a consequence of surplus star-forming material being stripped off by radiation and winds from nearby massive stars, leaving behind PMS stars away from molecular clouds.

3.5. *High Star Formation Efficiency*

Massive stars play a dual role in star formation. I-front compression may induce the birth of stars that otherwise could not have formed. Alternatively, molecular clouds may become highly disturbed, and hence dispersed, making subsequent star formation impossible. Even if triggered star formation is initiated, its operation is confined to the outer layers of a cloud. It is therefore expected that star formation may be efficient in localized, compressed regions, but perhaps not so in the entire cloud. The star formation efficiency (SFE) in a BRC can be estimated by the ratio of the stellar mass to the total mass of stars plus cloud. De Vries et al. (2002) observed the compressed regions of B35 and LDN 1634 in the HCO^+ molecular line and determined the total compressed mass of molecular clouds to be 27 $M_\odot$ for B35 and 28 $M_\odot$ for LDN 1634, respectively. We have identified three CTTSs in each of B35 and LDN 1634, so, assuming 0.5–1 $M_\odot$ for a typical CTTS, the SFEs of the compressed material in B35 and LDN 1634 are about 5%–10%, higher than those of a few percent (<3%) in other nearby star-forming regions (White et al. 1995).

4. CONCLUSIONS

We developed an empirical set of criteria to select candidate CTTSs on the basis of the infrared colors in the 2MASS Point Source Catalog. Among the 32 candidates for which we obtained spectra, 24 are found to be bona fide PMS objects, 4 are M-type stars, and the remaining 4 are carbon stars, which shows the effectiveness of our selection method. The young stellar population provides a tool to trace ongoing star formation activities. We find supportive evidence of triggered star formation in the following BRCs, B35, B30, IC 2118, LDN 1616, LDN 1634, and Ori East.

1. Our data supports the RDI model that links the formation of BRCs and of stars. According to this model the ionization fronts from OB stars compress a nearby cloud, and if the density of the compressed gas exceeds a certain critical value, new stars are formed. Not all BRCs are associated with CTTSs. Only BRCs associated with strong *IRAS* 100 μm emission (a tracer of high density) and Hα emission (a tracer of ionization front) show signs of ongoing star formation.

2. We find that CTTSs closer to BRCs are progressively younger, a configuration consistent with the sequential process of triggered star formation. The brightest CTTSs, spatially closest to BRCs, are the young stellar objects that just reveal themselves on the birth line and begin to descend down the Hayashi tracks.

3. The ages of the concurrent OB stars are comparable to or older than the ages of the next-generation stars plus the I-front traveling times. These timescales are consistent with the causality, or sequential, nature of the star formation process.

4. CTTSs are found only in between the OB stars and the molecular clouds with which the ionization fronts interact. There are no CTTSs ahead of the ionization fronts into the clouds. The lack of embedded CTTSs cannot be due to detection sensitivity because the extinction of these BRCs is generally low.

5. Current star formation in the BRCs takes place in the compressed outer layers of the molecular clouds. The relatively enhanced star formation efficiency suggests a triggered—as opposed to a spontaneous—star formation process.

This publication makes use of data products from the Two Micron All Sky Survey (2MASS), which is a joint project of the University of Massachusetts and the Infrared Processing and Analysis Center/California Institute of Technology, funded by the National Aeronautics and Space Administration and the National Science Foundation (NSF). We also use the Southern H-Alpha Sky Survey Atlas (SHASSA), supported by the NSF. We are grateful to the anonymous referee for helpful suggestions that improve the quality of this paper. We also thank the staff at the Beijing Astronomical Observatory for their assistance during our observing runs. H.-T. L. wants to thank Paul Ho for valuable discussions. We acknowledge the financial support of the grants NSC92-2112-M-008-047 of the National Science Council and 92-N-FA01-1-4-5 of the Ministry of Education of Taiwan.

REFERENCES

Bertoldi, F. 1989, ApJ, 346, 735
Bertoldi, F., & McKee, C. F. 1990, ApJ, 354, 529
Carpenter, J. M. 2001, AJ, 121, 2851
Cox, A. N. 2000, Allen's Astrophysical Quantities (4th ed.; New York: Springer)
De Vries, C. H., Narayanan, G., & Snell, R. L. 2002, ApJ, 577, 798
Dolan, C. J., & Mathieu, R. D. 2002, AJ, 123, 387
Duerr, R., Imhoff, C. L., & Lada, C. J. 1982, ApJ, 261, 135
Elmegreen, B. G. 1998, in ASP Conf. Ser. 148, Origins, ed. C. E. Woodward, J. M. Shull, & H. A. Thronson, Jr. (San Francisco: ASP), 150
Feigelson, E. D., & Montmerle, T. 1999, ARA&A, 37, 363
Finkbeiner, D. P. 2003, ApJS, 146, 407

Gaustad, J. E., McCullough, P. R., Rosing, W., & Van Buren, D. 2001, PASP, 113, 1326
Herbig, G. H., & Bell, K. R. 1988, Third Catalog of Emission-Line Stars of the Orion Population (Lick Obs. Bull. 1111; Santa Cruz: Lick Obs.)
Herbig, G. H., & Kameswara Rao, N. 1972, ApJ, 174, 401
Karr, J. L., & Martin, P. G. 2003, ApJ, 595, 900
Kenyon, S. J., Brown, D. I., Tout, C. A., & Berlind, P. 1998, AJ, 115, 2491
Lada, C. J. 1987, in IAU Symp. 115, Star Forming Regions, ed. M. Peimbert & J. Jugaku (Dordrecht: Reidel), 1
Lada, C. J., & Adams, F. C. 1992, ApJ, 393, 278
Lada, C. J., Muench, A. A., Haisch, K. E., Lada, E. A., Alves, J. F., Tollestrup, E. V., & Willner, S. P. 2000, AJ, 120, 3162
Lang, W. J., Masheder, M. R. W., Dame, T. M., & Thaddeus, P. 2000, A&A, 357, 1001
Lefloch, B., & Lazareff, B. 1994, A&A, 289, 559
———. 1995, A&A, 301, 522
Lefloch, B., Lazareff, B., & Castets, A. 1997, A&A, 324, 249
Levato, H., & Abt, H. A. 1976, PASP, 88, 712
Maddalena, R. J., Moscowitz, J., Thaddeus, P., & Morris, M. 1986, ApJ, 303, 375
Meyer, M. R., Calvet, N., & Hillenbrand, L. A. 1997, AJ, 114, 288
Ogura, K., & Sugitani, K. 1998, Publ. Astron. Soc. Australia, 15, 91
Oort, J. H., & Spitzer, L. J. 1955, ApJ, 121, 6
Rieke, G. H., & Lebofsky, M. J. 1985, ApJ, 288, 618
Schaerer, D., & de Koter, A. 1997, A&A, 322, 598
Schlegel, D. J., Finkbeiner, D. P., & Davis, M. 1998, ApJ, 500, 525
Schmidt-Kaler, T. 1982, Landölt-Bornstein, Group VI, Vol. 2, ed. K.-H. Hellwege (Berlin: Springer), 451
Siess, L., Dufour, E., & Forestini, M. 2000, A&A, 358, 593
Stanke, T., Smith, M. D., Gredel, R., & Szokoly, G. 2002, A&A, 393, 251
Sugitani, K., Fukui, Y., & Ogura, K. 1991, ApJS, 77, 59
Sugitani, K., & Ogura, K. 1994, ApJS, 92, 163
Thé, P. S., de Winter, D., & Pérez, M. R. 1994, A&AS, 104, 315
Walborn, N. R., & Panek, R. J. 1984, ApJ, 286, 718
White, G. J., Casali, M. M., & Eiroa, C. 1995, A&A, 298, 594
Wichmann, R., et al. 1996, A&A, 312, 439
Yonekura, Y., Hayakawa, T., Mizuno, N., Mine, Y., Mizuno, A., Ogawa, H., & Fukui, Y. 1999, PASJ, 51, 837
Zinnecker, H., Bastien, P., Arcoragi, J., & Yorke, H. W. 1992, A&A, 265, 726